Size-dependent impairment of cognition in mice caused by the injection of gold nanoparticles

2010 Nanotechnology 21 485102

(http://iopscience.iop.org/0957-4484/21/48/485102)

Nanotechnology **21** (2010) 485102 (9pp) doi:10.1088/0957-4484/21/48/485102

Size-dependent impairment of cognition in mice caused by the injection of gold nanoparticles

Yu-Shiun Chen[1], Yao-Ching Hung[2], Li-Wei Lin[3], Ian Liau[4], Meng-Yeng Hong[1] and G Steve Huang[1,5]

[1] Institute of Nanotechnology, Department of Materials Science and Engineering, National Chiao Tung University, 1001 University Road, Hsinchu 300, Taiwan, Republic of China
[2] Section of Gynecologic Oncology, Department of Obstetrics and Gynecology, China Medical University and Hospital, 91 Hsueh Shih Road, Taichung 404, Taiwan, Republic of China
[3] The School of Chinese Medicine for Post-Baccalaureate, I-Shou University, 8 Yida Road, Yanchao Township, Kaohsiung Country 82445, Taiwan, Republic of China
[4] Department of Applied Chemistry, National Chiao Tung University, 1001 University Road, Hsinchu 300, Taiwan, Republic of China

E-mail: gstevehuang@mail.nctu.edu.tw

Received 4 August 2010, in final form 4 October 2010
Published 4 November 2010
Online at stacks.iop.org/Nano/21/485102

Abstract

We explored the size-dependent impairment of cognition in mice caused by the injection of gold nanoparticles (GNPs). GNPs of 17 and 37 nm in diameter were injected intraperitoneally into BALB/c mice at doses ranging from 0.5 to 14.6 mg kg^{-1}. ICP-MS was performed on brain tissue collected 1, 14 and 21 days after the injection. A passive-avoidance test was performed on day 21. Monoamine levels were determined on day 21. The microscopic distribution of GNPs in the hippocampus was examined using coherent anti-Stokes Raman scattering (CARS) microscopy and transmission electron microscopy (TEM).

The results indicated that 17 nm GNPs passed through the blood–brain barrier more rapidly than 37 nm GNPs. Treatment with 17 nm GNPs decreased the latency time, which was comparable to the effect of scopolamine treatment, while 37 nm GNPs showed no significant effect. Dopamine levels and serotonin levels in the brain were significantly altered by the injection of 17 and 37 nm GNPs. GNPs affected dopaminergic and serotonergic neurons. CARS microscopy indicated that 17 nm GNPs entered the Cornu Ammonis (CA) region of the hippocampus, while 37 nm GNPs were excluded from the CA region. TEM verified the presence of 17 nm GNPs in the cytoplasm of pyramidal cells.

In this study, we showed that the ability of GNPs to damage cognition in mice was size-dependent and associated with the ability of the particles to invade the hippocampus. The dosage and duration of the treatment should be taken into account if GNPs are used in the future as vehicles to carry therapeutic agents into the brain.

S Online supplementary data available from stacks.iop.org/Nano/21/485102/mmedia

1. Introduction

Nanoparticles provide a novel platform for target-specific delivery of therapeutic agents [1–3]. Gold nanoparticles (GNPs) have recently been developed as an attractive candidate for use as carriers for drug and gene delivery because they possess several unique chemical and physical properties for the transportation and delivery of pharmaceuticals [4–7]. One principal advantage of these carriers is that the gold core is essentially inert and nontoxic. However, the toxicity of

[5] Author to whom any correspondence should be addressed.

these particles due to their small size has yet to be carefully examined.

The cytotoxicity of GNPs has previously been examined [8, 9], and GNPs may or may not be toxic to cell lines depending on the GNP size and surface modifications or the cell type used [10–15]. The cellular uptake of GNPs probably occurs through endocytosis and the largest amount of uptake occurs for 50 nm particles [16]. The size-dependent cellular uptake of GNPs was confirmed in a prostate cancer cell model [17]. Once particles enter cells, certain types of GNPs under 2 nm in diameter are toxic to many cell lines, while larger GNPs exhibit no toxic effects [18]. Although no apparent cytotoxicity has been found, GNP uptake has been associated with damage to the cytoskeleton and cell adhesion [19]. Alternatively, cytotoxicity of GNPs may be modified by coated materials [20]. For example, polyethylene glycol (PEG) coating greatly improves the biocompatibility and dispersion stability in an *in vitro* cell model [21].

The tissue distribution of GNPs in rats and mice has been examined *in vivo* by inductively coupled plasma mass spectrometry (ICP-MS) [22, 23]. GNPs of 10 nm in diameter were present in the liver, spleen, kidney, testis, thymus, heart, lung and brain, while GNPs larger than 50 nm were largely detected in the blood, liver and spleen. In particular, GNPs ranging from 10 to 50 nm were found in the brain. In another study, PEG-modified 13 nm GNPs accumulated in the liver and spleen for up to seven days after injection and induced acute inflammation and apoptosis in the liver [24]. The PEG-coated 20 nm GNPs showed significantly higher tumor uptake in a pharmacokinetics and biodistribution study of nude mice [25]. PEG-modified gold nanorods were found in the bloodstream and in the liver [26]. Another group observed that long-term retention of gold nanorods in the liver and spleen does not change the oxidation states of gold [27].

GNPs can pass through the blood–retinal barrier, but retinal toxicity was not observed [28]. It is important to investigate the physiological impact of naked GNPs once these particles enter the brain. This study will provide additional insight into the use of GNPs as carriers for drug delivery to the brain.

2. Materials and methods

2.1. Materials

$HAuCl_4$, sodium citrate, $NaBH_4$, HCl, HNO_3, H_2SO_4, H_2O_2 and other analytical grade chemicals were purchased from Sigma-Aldrich and Fisher in the United States. H_2O was obtained at >18 MΩ from a Milli-Q water purification system.

2.2. Preparation of gold nanoparticles

Gold nanoparticles (GNPs) with diameters of 17 and 37 nm were synthesized as previously reported [29, 30]. The seed colloids were prepared by adding 1 ml of 0.25 mM $HAuCl_4$ to 90 ml of H_2O and stirring for 1 min at 25 °C. A 2 ml volume of 38.8 mM sodium citrate was stirred into the solution for 1 min and then 0.6 ml of freshly prepared 0.1 M $NaBH_4$ in 38.8 mM sodium citrate was added. Different diameters of GNPs ranging from 3 to 100 nm were generated by changing the volume of seed colloid. The solution was stirred for an additional 5–10 min at 0–4 °C. The reaction temperatures and times were adjusted to obtain larger GNPs. All synthesized GNPs were characterized by UV absorbance. The size of the synthesized GNPs was verified by electron microscopy (supporting information, figure 1S, available at stacks.iop.org/Nano/21/485102/mmedia). The potential difference between the dispersion medium and the stationary layer of fluid attached to the dispersed GNPs was characterized by zeta potentials (table 1). Zeta potentials of both GNPs fell between ±40 and 60 mV, indicating good stability of the colloidal gold in the solution. GNPs were dialyzed against phosphate-buffered saline (pH 7.4) before injection to avoid toxicity from the buffer, such as endotoxins.

Table 1. Size distribution and zeta potentials of 17 nm (sample A) and 37 nm (sample B) GNPs. The size distribution and zeta potential of the gold nanoparticles was determined by a Delsa Nano C (NCTU Instruments Ltd, Hsinchu, Taiwan). The GNPs were resuspended in phosphate buffer (pH 7.4, 0.1 M) and the zeta potentials were measured at 25 °C.

Sample	Particle size (nm)	Zeta potential (mV)
A	17 ± 1.5	−45.9
B	37 ± 2.1	−47.8

2.3. Animal treatment

Animal treatments were performed following 'The Guidelines for the Care and Use of Experimental Animals' of the National Chiao Tung University in Taiwan. Four-week-old male BALB/c mice were housed at 22 ± 2 °C with a 12 h light/dark cycle and were fed standard rodent chow and water *ad libitum*. Mice were randomly assigned to four groups of 8–10 mice, including a control group consisting of mice that did not receive any treatment, a positive control that received scopolamine (1 mg kg^{-1} i.p.), a 17 nm GNP-treated group and a 37 nm GNP-treated group. GNPs were administered in a single dose intraperitoneally. A passive-avoidance test was performed on day 21 after the GNPs were administered. The animals were sacrificed at the end of the experiment by cervical dislocation, after which the brain was isolated and weighed. Excised tissue samples were washed with normal saline and stored at −70 °C for further assays.

Dose-dependent accumulation of GNPs was performed. GNPs at doses of 0.5 mg kg^{-1}, 0.9 mg kg^{-1}, 1.8 mg kg^{-1}, 3.7 mg kg^{-1}, 7.3 mg kg^{-1} and 14.6 mg kg^{-1} were administered. Animals were sacrificed on days 1, 14 and 21. The brain was isolated and weighed. ICP-MS was performed to obtain the concentration of gold accumulated in the brain.

2.4. Passive-avoidance test [31]

The apparatus consisted of two compartments with a steel-rod grid floor (supporting information, figure 2S (available at stacks.iop.org/Nano/21/485102/mmedia); 36 parallel steel rods, 0.3 cm in diameter, set 1.5 cm apart). One of the compartments (48 cm × 20 cm × 30 cm) was equipped with a 20 W lamp located in the center of the apparatus at a height of 30 cm and the other was a dark compartment of

the same size. The compartments were connected through a guillotine door (5 cm × 5 cm). The dark room was used during the experimental sessions that were conducted between 09:00 and 17:00 h. During the training trial, the guillotine door between the light and dark compartments was closed. When the mouse was placed in the light compartment with its back to the guillotine door, the door was opened and the time until the mouse entered the dark compartment (step-through latency, STL) was measured with a stopwatch. After the mouse entered the dark compartment, the door was closed. A 1 mA scrambled footshock was delivered through the grid floor for 2 s. The mouse was removed from the dark compartment 5 s after the shock. Then, the mouse was put back into the home cage until the retention trial was carried out 24 h later. The mouse was again placed in the light compartment and, similar to the training trial, the guillotine door was opened and the step-through latency was recorded. If the mouse did not step through the door after 300 s, the experiment was ended.

2.5. Analysis of monoamine and acetylcholine concentrations in the mouse brain

Monoamine levels were determined as previously reported [31]. The mice were decapitated and their brains were quickly removed. The brain samples were weighed and homogenized on ice using a Polytron homogenizer (Kinematica, Lucerne, Switzerland) at the maximum setting for 20 s in 10 volume equivalents of 0.2 M perchloric acid containing 100 mM Na_2-EDTA and 100 ng ml^{-1} isoproterenol. The homogenate was centrifuged at 15 000*g* for 30 min. The pH was adjusted to approximately 3.0 using 1 M sodium acetate. After filtration (0.45 μm), the samples were separated using high performance liquid chromatography (HPLC). Monoamines and their metabolites were separated using HPLC at 30 °C on a reverse-phase analytical column (ODS-80, 4.6 mm i.d. × 15 cm) and detected by an electrochemical detector (Model ECD-100, Eikom Co., Kyoto, Japan). The column was eluted with 0.1 M sodium acetate–citric acid buffer (pH 3.5) containing 15% methanol, 200 mg l^{-1} sodium 1-octanesulfonate and 5 mg l^{-1} Na_2-EDTA. The following monoamines and their metabolites were measured: norepinephrine (NE), 4-hydroxy-3-methoxyphenylglycol (MHPG), dopamine (DA), 3,4-dihydroxyphenylacetic acid (DOPAC), 5-hydroxytyramine (5-HT, serotonin) and 5-hydroxyindoleacetic acid (5-HIAA).

Acetylcholine (Ach) levels were determined as previously described [31]. The HPLC system (DSA-300, Eicom) consisted of a detector with a platinum electrode. A guard column and an enzyme column were placed before and after the analytical column (4.6 mm × 160 mm, Eicompak AC-GEL; Eicom), respectively. Isopropylhomocholine was added to the sampling tubes as an internal standard, and the mixture was analyzed using HPLC. The mobile phase was 0.1 M phosphate buffer (pH 8.3), and the flow rate was 0.6 ml min^{-1}. Ach levels in the sample were quantified by using the internal standard method.

2.6. Statistical analyses

All data are presented as mean ± SD with a minimum of six mice in each group. Concentrations of biogenic amines and Ach in the mouse brains were analyzed using an unpaired Student's *t*-test. The criterion for statistical significance was $p < 0.05$ for all statistical evaluations.

2.7. Inductively coupled plasma mass spectrometry (ICP-MS)

For the total element determinations, standard solutions were prepared by diluting a multi-element standard (1000 mg l^{-1} in 1 M HNO_3) obtained from Merck (Darmstadt, Germany). Nitric acid (65%), hydrochloric acid (37%), perchloric acid (70%) and hydrogen peroxide (30%) of Suprapur® grade (Merck) were used to mineralize the samples. A size-exclusion column was connected to the ICP-MS apparatus. Brain section samples were homogenized in 25 mM tris(hydroxymethyl)aminomethane (Tris)–12.5 mM HCl buffer solution at pH 8 and centrifuged at 13 000 rpm for 1 h. The supernatant was applied to the size-exclusion column of the HPLC system, which had been equilibrated with 25 mM Tris–12.5 mM HCl (containing 20 mM KCl) and eluted with the same buffer at a flow rate of 1 ml min^{-1}. The metal components of the metal-binding proteins that were eluted from the HPLC system were detected by ICP-MS (Perkin Elmer, SCIEX ELAN 5000). The operating conditions for the machine were as follows: RF power 1900 W, carrier gas flow 0.8 l min^{-1} Ar, and makeup gas flow 0.19 l min^{-1} Ar. ^{197}Au was used as the internal standard.

2.8. Ex vivo coherent anti-Stokes Raman scattering (CARS) microscopy

Freshly removed hippocampi were dissected into thin slices, approximately 2 mm in thickness, and immersed in a microchamber on a glass slide under PBS for examination. CARS microscopy was performed with a time constant of 3 ms, a scanning area of 300 μm × 300 μm, a step size of 1 μm, 300 pixels × 300 pixels, a scanning velocity of 1 μm ms^{-1} and a sampling rate of 80 kHz. The laser power was set at 30 mW for 870 nm and 40 mW for 1064 nm. The wavelengths of the pump and the Stokes lasers (Pump = 870 nm and Stokes = 1064 nm) were tuned to match a Raman shift (~2100 cm^{-1}) that falls in the so-called 'silent region' of the vibrational spectra of cells and tissues. As expected, the CARS images of the 'control' did not show appreciable contrast under the non-resonant condition, whereas the CARS signals were dramatically enhanced, i.e. they appeared as scattered bright spots on the images taken from the GNP-treated specimens. The enhancement presumably resulted from strong scattering by the GNPs and the large third-order polarizability of the GNPs [32–35].

2.9. Transmission electron microscopy (TEM)

Small pieces of unfixed tissue were fixed in 2.5% glutaraldehyde with 0.05 M sodium cacodylate-buffered saline (pH 7.4) at room temperature for 2 h. The primary fixation was followed by three 20 min washes with 0.05 M sodium cacodylate-buffered saline (pH 7.4). The samples were then placed into a 1% OsO_4 solution in the same buffer at room temperature for 1 h. OsO_4 fixation was followed by three

20 min distilled-water washes and dehydration in acetone. The samples were transferred to 33% and 66% Spurr resin/acetone solutions successively, with a 30 min incubation in each solution. Then, the samples were transferred to 100% Spurr resin, first for 5 h and then they were placed in fresh resin overnight. The samples were cut into 100 nm sections using an ultramicrotome. The grids with ultrathin sections were post-stained with uranyl acetate for 30 min followed by lead for 3 min. After the post-staining procedure, a thin layer of carbon was evaporated onto the grid surfaces. Ultrathin-sectioned material was examined with a JEOL 1400 and a 3200 FS TEM.

3. Results and discussion

3.1. Dose-dependent biodistribution of GNPs in mouse brain

GNPs (17 and 37 nm in diameter) were synthesized according to published procedures [29, 30]. The synthesis was monitored by UV absorbance, and the particle size was examined by electron microscopy (17 ± 1.5 nm and 37 ± 2.1 nm). The potential difference between the dispersion medium and the stationary layer of fluid attached to the dispersed GNPs was characterized by zeta potentials (table 1). Zeta potentials of both GNPs fell between ±40 and 60 mV, indicating good stability of the colloidal gold in the solution. The purified GNPs were injected intraperitoneally into the BALB/c mice at doses of 0.5–14.6 mg kg^{-1}. ICP-MS was performed on brains sampled at 1, 14 and 21 days after the injection to evaluate residual GNPs in the brain (figure 1). GNPs were detected in brain samples one day after the injection. GNPs accumulated rapidly in the first two weeks and continued to increase until the end of the third week. For all dosages, the amount of 17 nm GNPs deposited in the brain was approximately 20% higher than the amount deposited for 37 nm GNPs on days 1 and 14, while the levels were similar on day 21. It is likely that the 17 nm GNPs passed through the blood–brain barrier more readily than 37 nm GNPs, resulting in faster initial accumulation. However, the GNP levels were comparable on day 21. When the dosage of either GNP was higher than 7.3 mg kg^{-1}, symptoms of toxicity were noted in the mice at day 21. The treated animals showed fatigue, loss of appetite, changes in fur color and weight loss. Starting from day 21, the mice showed a significantly camel-like back and a crooked spine. These symptoms were consistent with previous results showing that high doses of GNPs induced multiple abnormalities in mice [36].

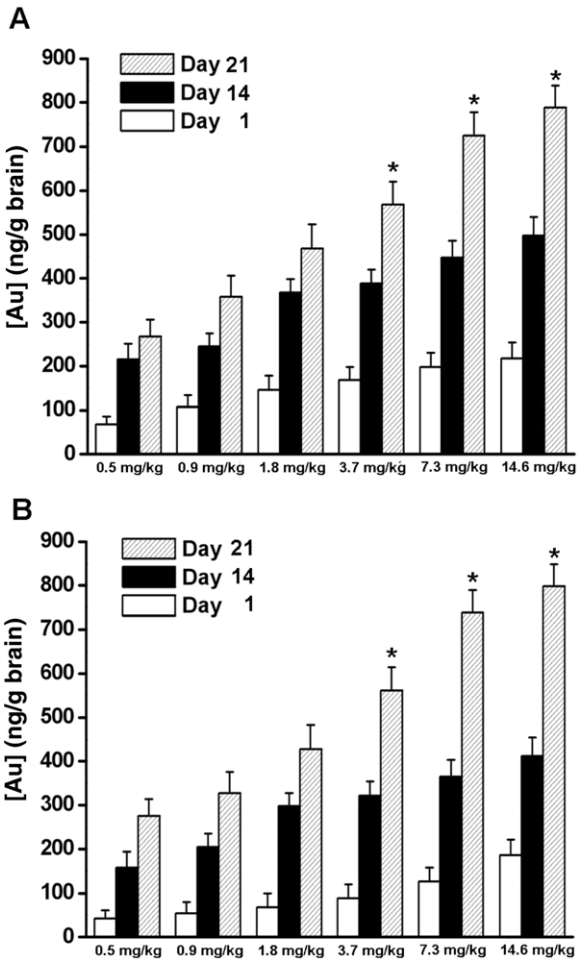

Figure 1. Accumulation of (A) 17 nm GNPs and (B) 37 nm GNPs in the brain. GNPs were injected intraperitoneally into mice at the indicated doses. Brain tissues were removed 1, 14 and 21 days after administering the GNPs. ICP-MS was performed to obtain the concentration of GNPs in brain tissue. Each value represents the average of six independent experiments and the error bars indicate standard deviation.

3.2. GNPs impair learning and memory in mice

To explore if the injected GNPs retarded brain function in mice, particularly learning and memory, we examined the passive-avoidance performance of GNP-treated mice at a GNP dose of 3.7 mg kg^{-1}. The dose was chosen as a minimal dose to avoid the lethal effect of GNPs. Previously, we demonstrated that the lethal dose of GNPs was 8 mg/kg/week for four consecutive weeks. However, the current study employed lower doses, which only caused minor symptoms in mice. Scopolamine has the potential to induce amnesia and was applied as the positive control (figure 2(A)). Untreated mice exhibited a latency of 180 ± 9 s. Scopolamine induced amnesia, resulting in an avoidance latency of 92 ± 22 s, a 50% reduction compared to the untreated controls ($p < 0.01$). Although both GNPs caused weakness in mice, an insignificant reduction in latency was observed for the 37 nm GNP-treated mice, while the 17 nm GNP-treated mice showed a latency of 81 ± 25 s in the passive-avoidance performance test ($p < 0.01$). The latency in the 17 nm GNP-treated mice was comparable to the amnesia caused by scopolamine treatment. Apparently, 17 nm GNPs cause amnesia in mice, while 37 nm GNPs have no effect.

A dose–response curve for various concentrations of 17 nm GNPs was obtained. The passive-avoidance test was performed on mice injected with 17 nm GNPs at doses of 0, 0.4, 0.8, 1.9, 3.7, 7.3 and 14.6 mg kg^{-1}. The lowest concentration of GNPs with a significantly reduced latency time (138 ± 10 s) compared to the control group was 1.9 mg kg^{-1} ($p < 0.05$). The concentrations below 1.9 mg kg^{-1} had no significant effects. The latency time

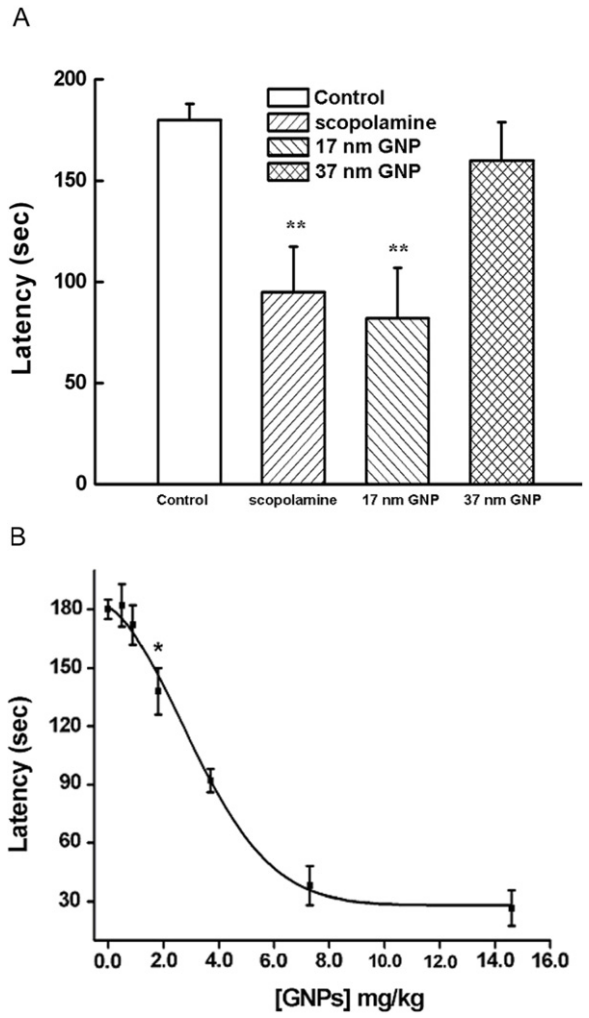

Figure 2. Learning impairment of passive-avoidance performance induced by scopolamine, 17 and 37 nm GNPs in mice. (A) Mice were randomly assigned to four groups, each containing 8–10 mice. The groups included a control group that did not receive any treatment, a positive control group that received scopolamine (1 mg kg^{-1} i.p.), the 17 nm GNP-treated group (3.7 mg kg^{-1}) and the 37 nm GNP-treated group (3.7 mg kg^{-1}). A passive-avoidance test was performed, and the averaged latency time is shown ($^{**}p < 0.01$). (B) Dosage response of mice injected with 17 nm GNPs in the passive-avoidance test. The passive-avoidance test was performed on mice injected with 17 nm GNPs at doses of 0, 0.4, 0.8, 1.9, 3.7, 7.3 and 14.6 mg kg^{-1}. The latency of the control group was 180 s. The lowest concentration of GNPs with a significantly reduced latency time (138 s) compared to control group was 1.9 mg kg^{-1} ($^{*}p < 0.05$). The concentrations below 1.9 mg kg^{-1} had no significant effects. The latency time at higher doses was dose-dependent and plateaued rapidly at 7.3 mg kg^{-1}.

at higher doses was dose-dependent and plateaued rapidly at 7.3 mg kg^{-1}.

3.3. The monoamine and acetylcholine concentration profiles in the mouse brain were significantly affected by GNPs

Formation and consolidation of learning and memory are associated with the activity of acetylcholinergic, norepinephrinergic, dopaminergic and serotonergic neurons [37]. Most of these neurotransmitter systems can influence learning and memory in mice. GNP-treatment induced learning impairment, which indicated that GNPs might cause an imbalance of neurotransmitters in the mouse brain (figure 3). Norepinephrine negatively regulates the learning and memory process [38]. However, administration of scopolamine, 17 nm GNPs and 37 nm GNPs did not affect the levels of norepinephrine and its metabolite MHPG. Activation of the dopaminergic system also causes learning impairment [39, 40]. GNP treatment elevated levels of dopamine from 114.5 ng g^{-1} brain to 143.6 ng g^{-1} brain for the 17 nm GNPs ($p < 0.01$), and to 138.2 for the 37 nm GNPs ($p < 0.05$). Serotonin was significantly reduced from 57.2 ng g^{-1} brain to 44.3 ng g^{-1} brain ($p < 0.05$) upon treatment with 17 nm GNPs [41]. Overall, GNP-induced learning impairment was correlated with an increase of dopamine and a decrease of serotonin in the mouse brain.

3.4. The macroscopic distribution of 17 and 37 nm GNPs in the brain were indistinguishable

The differential effects of 17 and 37 nm GNPs on the cognition of mice implied that the distribution of GNPs in the brain might be size-dependent. ICP-MS was used to detect the distribution of GNPs in the mouse brain. After 21 days of GNP injection at a dose of 3.7 mg kg^{-1}, mouse brains were dissected into six parts: the left and right frontal lobes, left and right medial temporal lobes, and the left and right occipital lobes. Both 17 and 37 nm GNPs were detected in all parts of the brain at concentrations ranging from 496.2 to 559.5 ng g^{-1} brain. The lowest concentration was found in the occipital lobes (figure 4). We were unable to differentiate the macroscopic distributions of 17 and 37 nm GNPs in the samples. The ICP-MS results indicated that 17 and 37 nm GNPs were capable of passing through the blood–brain barrier and entering the mouse brain.

3.5. CARS microscopy differentiated the local distributions of 17 and 37 nm GNPs in the hippocampus

The hippocampus is located in the medial temporal lobe of the brain, belongs to the limbic system and plays major roles in short-term memory as well as spatial navigation. Since GNP injection impaired learning and memory in mice, the GNPs could have been transported through the blood, across the blood–brain barrier into the brain and into the hippocampus. To verify the presence of GNPs, the freshly dissected hippocampi were observed using *ex vivo* CARS microscopy (figure 5). GNPs are known to enhance the anti-Stokes Raman signal of nearby amino acids. With proper controls, the enhancement made possible by CARS strongly indicated the presence of GNPs. GNPs were also diffused *ex vivo* into brain tissues to verify the enhancement of Raman signal. Localized enhancement of an anti-Stokes Raman signal at an excitation wavelength of 817 nm was observed from the hippocampi removed from 17 and 37 nm GNP-treated mice. The Raman signal was completely absent from control mouse tissues. The Raman signal of 17 nm GNPs was localized to the Cornu Ammonis (CA) region of the hippocampus inside a cluster of neuronal cells, while 37 nm GNPs were scattered

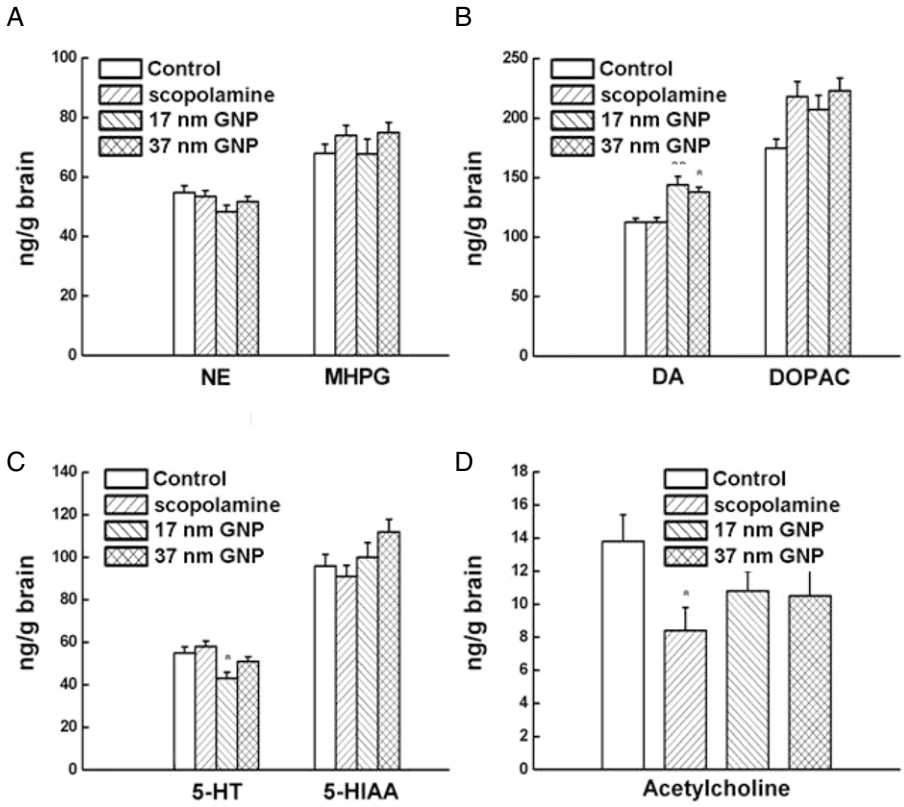

Figure 3. Fluctuation of monoamine and acetylcholine levels induced by scopolamine, 17 nm GNPs, and 37 nm GNPs in the mouse brain. Immediately after the passive-avoidance test, brain tissues were removed and levels of monoamines and acetylcholine were analyzed. The levels of neurotransmitters and their metabolites are shown in the plots. (A) Norepinephrine (NE) and 4-hydroxy-3-methoxyphenylglycol (MHPG). (B) Dopamine (DA) and 3,4-dihydroxyphenylacetic acid (DOPAC). (C) 5-hydroxytyramine (5-HT, serotonin) and 5-hydroxyindoleacetic acid (5-HIAA). (D) Acetylcholine. Each group of columns contains, in sequence, averaged values from the control group, the scopolamine-treated group, the 17 nm GNP-treated group and the 37 nm GNP-treated group. * indicates $p < 0.05$ and ** represents $p < 0.001$ from Student's t-test.

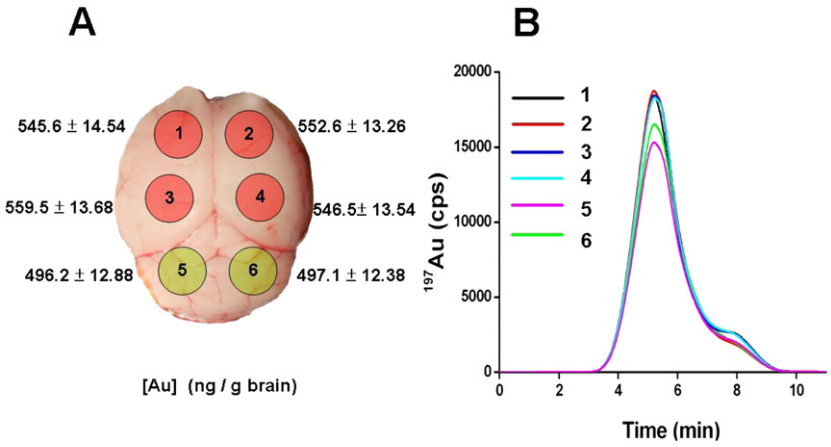

Figure 4. Global distribution of 17 nm GNPs in the mouse brain. (A) Schematic representation of the six areas dissected from the mouse brain and the corresponding 17 nm GNP concentrations based on the results of ICP-MS detection. These values represent the average of six independent experiments. (B) ICP-MS readings for typical samples were obtained from each part of the brain.
(This figure is in colour only in the electronic version)

throughout the peripheral region. The distribution of 17 and 37 nm GNPs in the hippocampus suggested that the invasion of GNPs into the cluster of neuronal cells in the CA might have caused learning impairment in the 17 nm GNP-treated mice, while the 37 nm GNPs were incapable of entering neuronal cells and only caused minimal deficits in learning and memory.

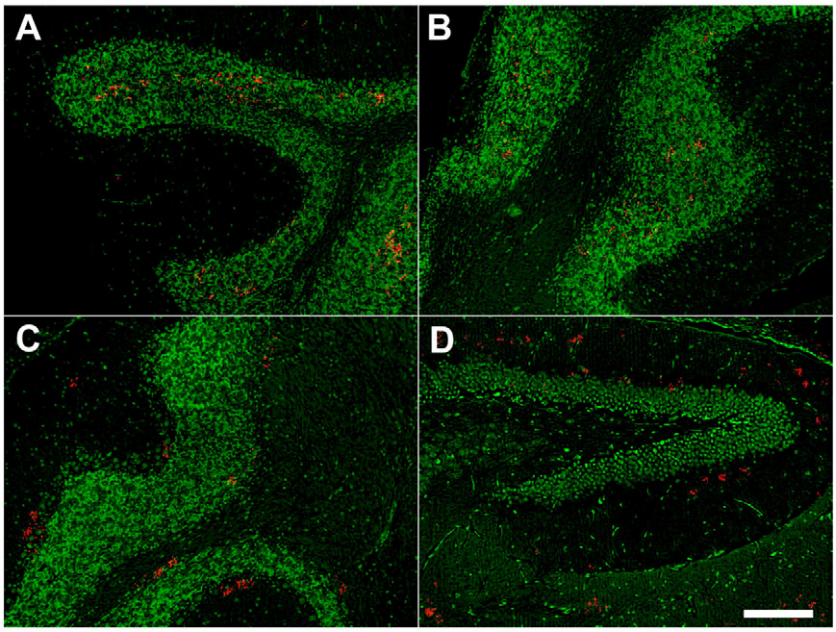

Figure 5. CARS microscopy of hippocampi isolated from 17 nm GNP-treated and 37 nm GNP-treated mice. The wavelengths of the pump and the Stokes lasers (Pump = 870 nm and Stokes = 1064 nm) were tuned to match a Raman shift ($\sim$2100 cm^{-1}) that fell in the so-called 'silent region' of the vibrational spectra of cells and tissues. To better visualize the location of GNPs, the enhanced bright spots are red in the final images. The green fluorescence is the auto-fluorescence emitted from the cells of the CA region in the hippocampus. (A), (B) Hippocampi obtained from 17 nm GNP-treated mice. (C), (D) Hippocampi obtained from 37 nm GNP-treated mice. Scalebar = 200 μm.

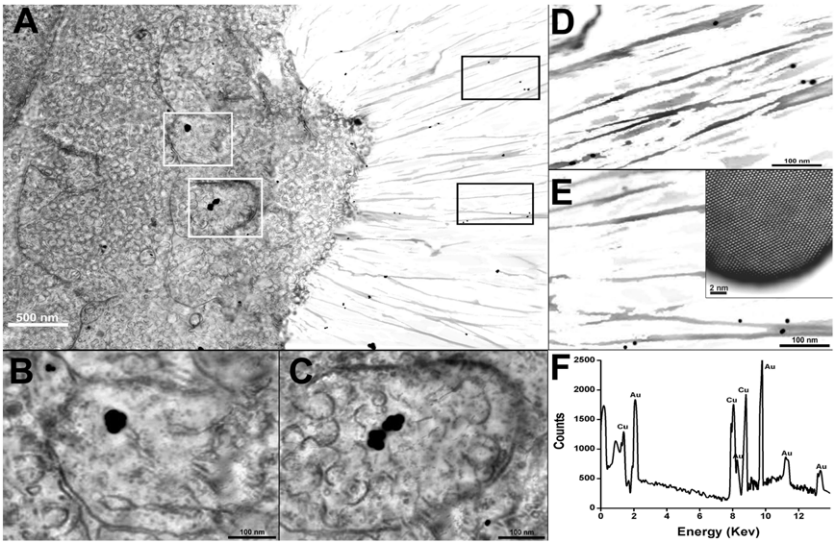

Figure 6. TEM images of neuronal cells from the hippocampus of a 17 nm GNP-treated mouse. (A) Entire view. (B), (C) Enlarged areas from (A) showing the invasion of 17 nm GNPs and the surrounding coated pit-like structures in the cytoplasm. (D) Enlarged area from (A) showing the association of GNPs with the dendrites. (E) is similar to (D) but contains an inset HR-TEM image showing the metallic nature of the black spots. (F) EDS of the selected GNPs in (B).

3.6. TEM revealed that 17 nm GNPs were located in the cytoplasm of hippocampal neurons while 37 nm GNPs were not

TEM was performed to verify the cytoplasmic location of the 17 and 37 nm GNPs in the hippocampus 21 days after the injection of GNPs (figures 6 and 7). A total of 72 TEM images were examined. We found that the 17 nm GNPs were located in the cytoplasm of pyramidal cells (figures 6(A)–(C)). The Au composition was verified using energy dispersive x-ray spectroscopy (EDS; figure 6(F)), and the gold was also detected using HR-TEM (figure 6(E)). The 17 nm GNPs were found to be associated with dendrites (figure 6(D)). In particular, the 17 nm GNPs were surrounded by coated pit-like structures in the cytoplasm, leading us to suspect that the 17 nm GNPs entered the cells through endocytosis. However, no endocytosis-related structures were found for the 17 nm

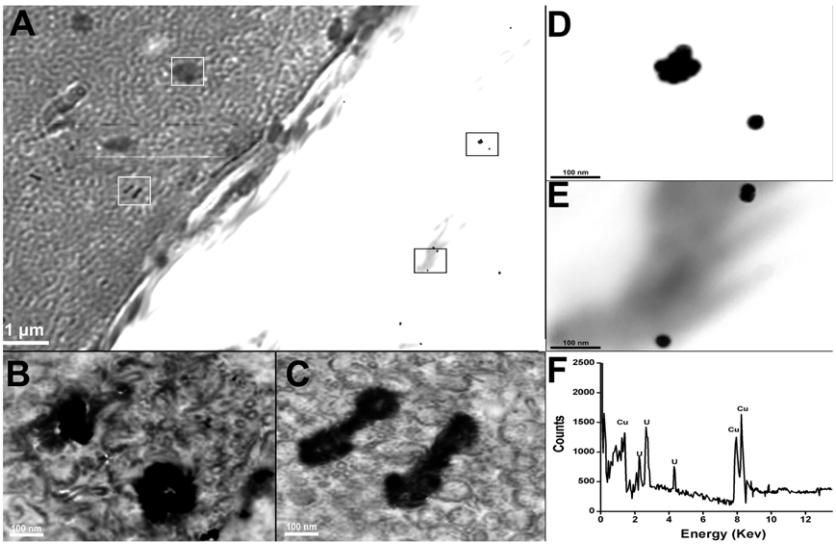

Figure 7. TEM images of neuronal cells from the hippocampus of a 37 nm GNP-treated mouse. (A) Entire view. (B), (C) Enlarged areas from (A) showing the dark spots. (D), (E) Enlarged areas from (A) showing the association of GNPs with dendrites. (F) EDS of the dark spots in (B) identifies these spots as uranium.

GNPs at the dendrites. This result implies that these GNPs entered the dendrites through free diffusion. Additionally, these results suggest that alternative mechanisms for the cell uptake of GNPs occur together as previously reported. The invasion of metallic particles, such as GNPs, into neuronal cells and dendrites could seriously interfere with electric signals transmitted through the hippocampus, thereby inducing learning and memory impairments.

The presence of 37 nm GNPs in the hippocampus was also examined by TEM (figure 7). Several dark spots were noted in the cytoplasm of neuronal cells (figures 7(A)–(C)). Further examination with EDS revealed that these spots were composed of uranium, possibly due to the heterogeneity of the staining solution (figure 7(F)). Many 37 nm GNPs were detected inside the dendritic structure of brain cells. However, no endocytic structures were associated with 37 nm GNPs in the dendrites. Apparently, the 37 nm GNPs that entered dendrites through free diffusion were excluded from the cell bodies.

There, evidence overwhelming showed that GNPs have negligible toxicity in cultured cells. The *in vivo* biodistribution has been determined in mice and rats. However, no further evidence regarding the physiological impact in animals has been provided. In zebrafish, GNPs exhibited minimal *in vivo* toxicity with an embryo mortality less than 3%, while silver nanoparticles showed an almost 100% mortality. The difference in toxicity between gold and silver was due more to the unique chemistry of silver and less to a simple reduction in size. If the gold nanoparticles showed any size-dependent toxicity, this toxicity would be mild and the particles would be better tolerated than silver nanoparticles. For this reason, the delicate functions of the brain provided an opportunity to prove this hypothesis. These results showed that the injection of seemingly nontoxic GNPs can impair the learning and memory of mice at a sufficient dose. The reduction of cognitive ability was associated with the endocytosis of 17 nm GNPs into the neuronal cells in the CA region of the hippocampus. The observation that 37 nm GNPs were found in the extracellular region of the hippocampus was consistent with the inability of the GNPs to impair cognition in mice.

The differential effect of 17 and 37 nm GNPs on the cognition of mice indicated that physical diffusion could be a key process. The day 1 and day 14 dose–brain accumulation curves indicated that 17 nm GNPs crossed the blood–brain barrier faster than 37 nm GNPs (figure 1). The macroscopic biodistribution of the two GNPs within the brain were indistinguishable from one another. However, the monoamine and acetylcholine profiles were comparable. The microscopic evidence implied that 17 nm GNPs entered into the brain tissue and diffused faster than 37 nm GNPs. In CARS, the Raman signal of 17 nm GNPs was localized to the CA regions of the hippocampus inside the cluster of neuronal cells, while 37 nm GNPs were scattered through the peripheral region. The distribution of 17 and 37 nm GNPs in the hippocampus implied that the invasion of GNPs into a cluster of neuronal cells in the CA might have caused learning impairment in the 17 nm GNP-treated mice. In contrast, 37 nm GNPs were unable to enter neuronal cells, and therefore caused only minimal deficits in learning and memory. The difference in the effects on cognition of the two GNPs was apparently caused by the difference in cell entry. Although both GNPs caused a global fluctuation in neurotransmitter levels in the brain, the differences in their invasive ability into the hippocampus determined the fate of the mice.

Binding of citrate at the gold surface was dynamic. It is possible that surface modifications that could have replaced citrate on the GNPs could have occurred after injection. Proteins such as albumin, immunoglobulins, complement, fibrinogen and apolipoproteins bind strongly to nanoparticles once the particles are in body fluids [42]. In particular, binding between complement and immunoglobulin (opsonization) promotes receptor-mediated phagocytosis [43, 44]. Binding

of plasma protein is important for determining the *in vivo* biodistribution of nanoparticles. This binding might explain how the injected GNPs passed through the blood–brain barrier and entered into the hippocampus.

The brain is the most delicate and complex organ in animals. Both GNPs in this study affected monoamine profiles in the brain, indicating that brain functions other than learning and memory might be affected by the injection of GNPs. The invading GNPs could also have caused the abnormal transmission of electrical signals through neurons. It is also possible that the engulfment of GNPs may induce an abnormal cellular response, such as apoptosis or an imbalance of intracellular electrolytes. Further experiments are necessary to explore the extent of the damaging effects of GNPs.

4. Conclusions

This study showed that the invasion of seemingly nontoxic GNPs can impair learning and memory in mice. The reduction in cognitive ability was associated with the endocytosis of 17 nm GNPs into neurons of the CA regions of the hippocampus. While GNPs have been widely used for targeting and imaging in drug delivery, this study provided additional insight into the design of drug carriers that deliver molecules to specific areas of the brain.

Acknowledgments

This study was supported in part by the National Science Council of Taiwan (grant NSC94-2320-B-009-003) and by the Aim for the Top University Plan of the National Chiao Tung University and the Ministry of Education in Taiwan.

References

[1] Ferrari M 2005 *Nat. Rev. Cancer* **5** 161–71
[2] Olivier J C 2005 *NeuroRx* **2** 108–19
[3] Yih T C and Al-Fandi M 2006 *J. Cell. Biochem.* **97** 1184–90
[4] Ghosh P, Han G, De M, Kim C K and Rotello V M 2008 *Adv. Drug Deliv. Rev.* **60** 1307–15
[5] T S Hauck, A A Ghazani and W C Chan 2008 *Small* **4** 153–9
[6] Paciotti G F, Myer L, Weinreich D, Goia D, Pavel N, McLaughlin R E and Tamarkin L 2004 *Drug Deliv.* **11** 169–83
[7] Rosi N L, Giljohann D A, Thaxton C S, Lytton-Jean A K, Han M S and Mirkin C A 2006 *Science* **312** 1027–30
[8] Connor E E, Mwamuka J, Gole A, Murphy C J and Wyatt M D 2005 *Small* **1** 325–7
[9] Shukla R, Bansal V, Chaudhary M, Basu A, Bhonde R R and Sastry M 2005 *Langmuir* **21** 10644–54
[10] Goodman C M, McCusker C D, Yilmaz T and Rotello V M 2004 *Bioconjug. Chem.* **15** 897–900
[11] Khan J A, Pillai B, Das T K, Singh Y and Maiti S 2007 *ChemBioChem* **8** 1237–40
[12] Male K B, Lachance B, Hrapovic S, Sunahara G and Luong J H 2008 *Anal. Chem.* **80** 5487–93
[13] Murphy C J, Gole A M, Stone J W, Sisco P N, Alkilany A M, Goldsmith E C and Baxter S C 2008 *Acc. Chem. Res.* **41** 1721–30
[14] Patra H K, Banerjee S, Chaudhuri U, Lahiri P and Dasgupta A K 2007 *Nanomedicine* **3** 111–9
[15] Takahashi H, Niidome Y, Niidome T, Kaneko K, Kawasaki H and Yamada S 2006 *Langmuir* **22** 2–5
[16] Chithrani B D, Ghazani A A and Chan W C 2006 *Nano Lett.* **6** 662–8
[17] Malugin A and Ghandehari H 2010 *J. Appl. Toxicol.* **30** 212–7
[18] Pan Y, Neuss S, Leifert A, Fischler M, Wen F, Simon U, Schmid G, Brandau W and Jahnen-Dechent W 2007 *Small* **3** 1941–9
[19] Pernodet N, Fang X, Sun Y, Bakhtina A, Ramakrishnan A, Sokolov J, Ulman A and Rafailovich M 2006 *Small* **2** 766–73
[20] Qiu Y, Liu Y, Wang L, Xu L, Bai R, Ji Y, Wu X, Zhao Y, Li Y and Chen C 2010 *Biomaterials* **31** 7606–19
[21] Rayavarapu R G, Petersen W, Hartsuiker L, Chin P, Janssen H, van Leeuwen F W, Otto C, Manohar S and van Leeuwen T G 2010 *Nanotechnology* **21** 145101
[22] De Jong W H, Hagens W I, Krystek P, Burger M C, Sips A J and Geertsma R E 2008 *Biomaterials* **29** 1912–9
[23] Sonavane G, Tomoda K and Makino K 2008 *Colloids Surf.* B **66** 274–80
[24] Cho W S, Cho M, Jeong J, Choi M, Cho H Y, Han B S, Kim S H, Kim H O, Lim Y T and Chung B H 2009 *Toxicol. Appl. Pharmacol.* **236** 16–24
[25] Zhang G, Yang Z, Lu W, Zhang R, Huang Q, Tian M, Li L, Liang D and Li C 2009 *Biomaterials* **30** 1928–36
[26] Niidome T, Yamagata M, Okamoto Y, Akiyama Y, Takahashi H, Kawano T, Katayama Y and Niidome Y 2006 *J. Control. Release* **114** 343–7
[27] Wang L, Li Y F, Zhou L, Liu Y, Meng L, Zhang K, Wu X, Zhang L, Li B and Chen C 2010 *Anal. Bioanal. Chem.* **396** 1105–14
[28] Kim J H, Kim K W, Kim M H and Yu Y S 2009 *Nanotechnology* **20** 505101
[29] Brown K R, Walter D G and Natan M J 2000 *Chem. Mater.* **12** 306–13
[30] Liu F-K, Ker C-J, Chang Y-C, Ko F-H, Chu T-C and Dai B-T 2003 *Japan. J. Appl. Phys.* **42** 4152–8
[31] Hsieh M T, Wu C R and Hsieh C C 1998 *Pharmacol. Biochem. Behav.* **60** 337–43
[32] Addison C J, Konorov S O, Brolo A G, Blades M W and Turner R F B 2009 *J. Phys. Chem.* C **113** 3586–92
[33] Evans C L, Potma E O, Puoris'haag M, Cote D, Lin C P and Xie X S 2005 *Proc. Natl Acad. Sci. USA* **102** 16807–12
[34] Hayazawa N, Ichimura T, Hashimoto M, Inouye Y and Kawata S 2004 *J. Appl. Phys.* **95** 2676–81
[35] Qian X, Peng X-H, Ansari D O, Yin-Goen Q, Chen G Z, Shin D M, Yang L, Young A N, Wang M D and Nie S 2008 *Nat. Biotechnol.* **26** 83–90
[36] Chen Y-S, Hung Y-C, Liau I and Huang G S 2009 *Nanoscale Res. Lett.* **4** 858–64
[37] Myhrer T 2003 *Brain Res. Brain Res. Rev.* **41** 268–87
[38] Thomas S A and Palmiter R D 1997 *Behav. Neurosci.* **111** 579–89
[39] Denenberg V H, Kim D S and Palmiter R D 2004 *Behav. Brain Res.* **148** 73–8
[40] Spanagel R and Weiss F 1999 *Trends Neurosci.* **22** 521–7
[41] Ogren S O, Eriksson T M, Elvander-Tottie E, D'Addario C, Ekstrom J C, Svenningsson P, Meister B, Kehr J and Stiedl O 2008 *Behav. Brain Res.* **195** 54–77
[42] Nel A E, Madler L, Velegol D, Xia T, Hoek E M, Somasundaran P, Klaessig F, Castranova V and Thompson M 2009 *Nat. Mater.* **8** 543–57
[43] Dobrovolskaia M A and McNeil S E 2007 *Nat. Nanotechnol.* **2** 469–78
[44] Owens D E III and Peppas N A 2006 *Int. J. Pharm.* **307** 93–102